



Research Article

Measurement of the flow behavior index of Newtonian and shear-thinning fluids via analysis of the flow velocity characteristics in a mini-channel

Shadi Ansari¹ · Md. Ashker Ibney Rashid¹ · Prashant R. Waghmare¹ · David S. Nobes¹ 

Received: 20 June 2020 / Accepted: 21 September 2020 / Published online: 8 October 2020
© Springer Nature Switzerland AG 2020

Abstract

An *in-situ* measurement technique to determine the rheology of a fluid based on the experimentally measured velocity profile of a flow in a mini-channel is introduced. The velocity profiles of a Newtonian and different shear-thinning fluids along a rectangular channel were measured using shadowgraph particle image velocimetry (PIV). Deionized water and different concentrations of a polyacrylamide solution were used as Newtonian and shear-thinning fluids, respectively and were studied at different Reynolds numbers. The flow indices of the fluids were determined by comparing the experimental velocity profile measurements with developed theory that takes into account the non-Newtonian nature of the fluids rheology. The results indicated that the non-Newtonian behavior of the shear-thinning fluid intensified at lower Reynolds numbers and it behaved more as a Newtonian fluid as the Reynolds number increased. A comparison between the power law index determined from experimental monitoring of the velocity profile at different Reynolds numbers and measurements from a rheometer reflected good agreement. The results from the study validate the new approach of the rheology measurement of Newtonian and non-Newtonian flows through straight, rectangular cross-section channels. The proposed approach can be further utilized using other methods such as X-ray PIV to characterize the rheology of non-transparent fluids and in general, for all non-Newtonian fluids.

Keywords Velocity profile · Mini-channel flow · Rheological properties · Non-newtonian flow · PIV

1 Introduction

In industrial applications for efficient transport of fluids or characterizing the motion of carried materials such as microorganisms in biological application [1] or components in drug delivery [2], a clear understanding of the carrying fluid's rheology is needed [3]. The rheology of the fluid determines the flow parameters such as flow velocity and pressure field. Knowledge of rheological properties of the fluid flow behavior helps to obtain better understanding of the resultant pumping energy required for fluid transport [4], the energy required to transport the material [5] or the potential locations of the material deposition in a flow passage [6]. Hence, the quantification of

rheological properties of the fluid in a continuous manner would be beneficial to understand the flow phenomena both for a single-phase flow or for flows carrying suspended particles.

Ex-situ rheological measurement techniques, such as a rotational rheometer [7] are currently the conventional approach for quantifying the rheological properties of the fluid. In these measurements, the bulk rheology of the fluid is measured by variation of shear rate and the shear stress applied on the sample collected. These methods have their own advantage and a number of important limitations need to be considered. First, these techniques usually requires general information on the rheological properties of the fluid to have a proper range of applied shear

✉ David S. Nobes, david.nobes@ualberta.ca | ¹Department of Mechanical Engineering, University of Alberta, Edmonton, Canada.



rate for fluids having low and high viscosities. The range of the shear rate that can be applied to the fluid is also limited to the type of rheometer and the exact shear rate through the geometry of an application such as a micro-channel cannot be provided using a classical rheometer. In addition, the effect of geometry of the channel is not accounted as the test fluid is needed to be removed from the flow geometries which in some cases are difficult to apply or they do not represent the application conditions [8]. Using a commercial rheometer can be also challenging and costly to study fluid flow at boundaries and where the measurement needs to be carried out at high temperatures and pressures [9].

The capability of an ex-situ rheological method can be limited for some applications. In the case of flow through micro and nano systems, e.g. flow in biological systems [10], rheological measurement using a traditional rheometer is challenging as only a small amount of the test fluid is available. The utilization of an ex-situ measurement is also limited for applications operating at high pressure and temperatures, e.g. the rheology of bitumen in SAGD process [11]. The rheology of the fluid flowing through different channels at various conditions as per the application could therefore be identified using a non-intrusive method for in-situ rheological measurement [12–14]. These issues highlight the potential, if a new method can be developed so that no prior knowledge of the fluid's properties is needed to determine the rheology of the fluid.

Studies have shown that the rheology of a liquid has a significant effect on the shape of the fully developed velocity profile of the fluid passing through different geometric channels [15–19]. The velocity gradient resulting from the interacting effects from the fluid rheology and flow conditions are strongly dependent on the shear rate and shear stress in the flow domain. These result in the velocity profile having strongly different shapes of a top-hat, plug-like, parabolic or a sharp-pointed on the center-line of the flow depending on the nature of the fluid and its flow geometry [16]. Therefore, the rheology of the fluid can be determined from a field measurement of velocity.

The rheological properties of a liquid that are determined by shear rate can be described using different rheological models including the Herschel-Bulkley, Ostwald [20], Carreau-Yasuda [17], Bingham model [21], Kundu and Cohen [22] and Tropea et al. [23]. Among all approaches used to describe the rheological behaviors of Newtonian and non-Newtonian fluids that do not exhibit a yield stress property, Ostwald-de Waele's power law approach is the simplified model widely being used by engineers [20, 24]. In this model, the relationship between shear rate and shear stress is described as a function of a power law index (n) and the flow consistency (k) of the fluid. The rheology

can be described by the power law index to classify the fluid as Newtonian ($n = 1$) or non-Newtonian ($n \neq 1$). This model has its limitation for the rheological calculation. The simplicity of the model, however, makes it more convenient to determine the rheology of a power law fluid.

Based on studies on a fluid's characteristics [25, 26], quantification of the rheology of the fluid can be achieved by coupling the velocity profile and corresponding theory. This enables the identification of the rheology of (even) an unknown fluid from the measurement of its velocity profile. The literature contains a number of works that have highlighted the measurement of the velocity profile for different Newtonian and non-Newtonian flows and their corresponding theory [15–19, 27]. One of the introduced methods using the velocity profiles to determine rheology of the fluid is the combination of the ultrasound-Doppler velocity profiling technique and pressure difference technology (UVP-PD) [28, 29]. A considerable amount of literature has been published on the application of this method discussing the capability for the rheological measurement of different fluids [9, 29–31]. However, there are certain drawbacks associated with the use of this method such as the sensitivity of the rheological measurements on the inclination angle of the transducers and the pulse frequency. These methods are inline and non-intrusive, but the measurement is limited to the location where the transducers are mounted (flow adapter cell) and cannot be applied for different locations along the fluid flow [29]. Therefore, to have a rheological measurement of any type of application, a non-intrusive methodology needs to be introduced that is capable of characterizing the rheological properties of a power law fluid at any location along the flow, pressure and temperature of the application.

Optical measurement techniques are the main non-intrusive methods that can be used to determine the velocity distribution of a fluid. Particle shadow velocimetry (PSV) can be selected as the measuring technique which is capable of measuring velocity profiles as well as identifying flow structures [32–34]. In this technique, the velocity of the flow within the region-of-interest is measured by determining the displacement of tracer particles that are added to the transparent fluid [35] such that the rheology of the fluid is not affected. The velocity measurement can be undertaken in wide range of flow rates and flow geometry which increases the range of the rheological measurement. Although the current method, PSV for velocity measurement can be used for a transparent fluid, application of the method could be extended for velocity measurement within translucent and opaque fluids [36–41] by using appropriate PIV techniques such as X-ray PIV.

The aim of this paper is to introduce a methodology to evaluate the flow behavior index of Newtonian and shear-thinning fluid based on velocity measurements. A

mathematical model that allows the rheology of the fluid to be determined from the velocity profile of the flow within a mini-channel is first illustrated. The velocity distributions for both Newtonian and shear-thinning (non-Newtonian) flows along a mini-channel are then experimentally investigated using shadowgraph PIV. Measured velocity profiles are compared with the corresponding mathematical model to determine the rheological parameters of the fluid. Rheological measurements are also collected using a standard rheometer to compare with the results from the proposed technique. The work concludes with a discussion of the results highlighting the feasible application of the introduced measurement approach.

2 Theory of Newtonian and non-Newtonian fluid through mini-channels

The velocity distribution and shape of the profile of laminar flows of Newtonian and non-Newtonian flows in mini channels has been well established [15, 16, 18]. The velocity distribution of a flow and the shape of its profile depend on the fluid rheology, Reynolds number and the position along the channel. The rheology of a fluid can be described by the measured variation in shear rate and viscosity of the fluid as the shear stress changes. Using the Ostwald-de Waele power law model and a definition of the flow shown in Fig. 1, the relationship of the viscosity, shear rate and shear stress of the fluid can be determined as a function of characteristic indices using:

$$\mu = k \left(\frac{\partial u}{\partial y} \right)^{n-1} \tag{1}$$

$$\tau = k \dot{\gamma}^n \tag{2}$$

where τ is shear stress, $\dot{\gamma}$ is shear rate defined as $\frac{\partial u}{\partial y}$, μ is viscosity, k is the flow consistency index and n is the power law index of the fluid. The value of the power law index, n , describes the rheology of the fluid where for Newtonian fluids $n = 1$ and $n \neq 1$ represents non-Newtonian fluids. The values of the flow indices indicate that for Newtonian fluid

there is a linear relationship between shear rate and shear stress. For non-Newtonian fluids, a nonlinear relationship could be expected. It can be also concluded that as the applied shear rate changes, the viscosity of a Newtonian fluid remains constant while the viscosity of a non-Newtonian fluid varies with shear rate.

To study the flow of Newtonian and non-Newtonian fluids through a rectangular mini-channel, a channel with width of h as shown in Fig. 1 was chosen as the flow domain. The flow enters the channel with a constant velocity of u and after traversing a certain length of the channel, the entrance length, L_h it becomes fully developed. The entrance length of a circular channel required for a laminar flow to become fully developed can be calculated as [22]:

$$L_h = 0.06 Re \cdot D_h \tag{3}$$

where Re is the Reynolds number and D_h is the hydraulic diameter of the channel. For the case of power law fluids, the Reynolds numbers can be calculated as [42]:

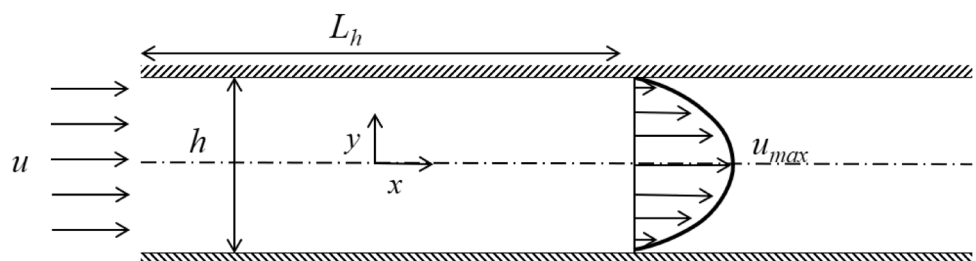
$$Re = \frac{\rho D_h^n u^{2-n}}{k} \left(\frac{n}{a + bn} \right)^n 8^{1-n} \tag{4}$$

where ρ is the fluid density, u is the average velocity of the fluid calculated in the fully developed region and a and b are constants which depend on the cross section of the channel. For circular pipes $a = 0.25$ and $b = 0.75$ and for square channels $a = 0.2121$ and $b = 0.6766$ [42]. For the case of a Newtonian fluid since $n = 1$ and $k = \mu$, the Reynolds number of the fluid can be simplified to:

$$Re = \frac{\rho D_h u}{\mu} \tag{5}$$

The velocity distribution of Newtonian and non-Newtonian fluids through the domain can be compared in the fully developed region where the boundaries of the fluid extend to the centerline of the channel. In this region, the maximum velocity of the fluid occurs at the centerline of the channel and the no-slip boundary condition applies at the walls. The velocity distribution of the fully developed region can be determined using the momentum conservation equation using the flow/geometry definition given in Fig. 1 as:

Fig. 1 Schematic of fully developed flow passing through a rectangular channel



$$\rho \left(\frac{\partial u}{\partial t} + u \frac{\partial u}{\partial x} + v \frac{\partial u}{\partial y} + w \frac{\partial u}{\partial z} \right) = -\frac{dp}{dx} + \frac{\partial}{\partial x}(\tau_{xx}) + \frac{\partial}{\partial y}(\tau_{xy}) + \frac{\partial}{\partial z}(\tau_{xz}) + \rho g \tag{6}$$

where $u, v,$ and w are the velocity components; τ_{xx}, τ_{xy} and τ_{xz} are shear rates in the channel in axial directions, p is pressure; and g is gravity. To study the velocity profile of Newtonian and non-Newtonian fluids, power law fluids with constant density along the channel were selected as a case of study and the flow is assumed to be in the x -direction only with no gravitational effects. Using these conditions, the momentum conservation equation for the case of steady state, fully developed and incompressible fluids simplifies to:

$$-\frac{dp}{dx} + \frac{\partial}{\partial x}(\tau_{xx}) + \frac{\partial}{\partial y}(\tau_{xy}) + \frac{\partial}{\partial z}(\tau_{xz}) = 0 \tag{7}$$

where τ_{xx} and τ_{xz} are equal to zero since it is assumed that for laminar flow the velocity of the fluid is only in the x -direction. For the fluid, τ_{xy} can also be determined from the power law model represented in Eq. (2). Applying the values of shear rates in different directions to Eq. (7), the velocity profile in the flow x -direction for a power law fluid across the cross section of a channel will simplify to:

$$-\frac{dp}{dx} + \frac{\partial}{\partial y} \left(k \left(\frac{\partial u}{\partial y} \right)^n \right) = 0 \tag{8}$$

The velocity of a power law fluid across the cross section of a channel can be calculated by integrating Eq. (8) with respect to y to give:

$$k \left(\frac{du}{dy} \right)^n = y \frac{dp}{dx} + c_1 \tag{9}$$

where c_1 is the constant of integration. At the center of the channel ($y = 0$), the velocity of the fluid reaches its maximum and $\frac{\partial u}{\partial y} = 0$ which leads to $c_1 = 0$. The resulting equation gives the relationship between the velocity gradient of the fluid with the pressure drop along the channel. The velocity profile of the fluid with respect to position in y -direction can then be determined by integrating Eq. (9) to give:

$$u = \frac{\left(\frac{y}{k} \frac{dp}{dx} \right)^{\frac{1}{n}+1}}{\frac{1}{k} \frac{dp}{dx} \left(\frac{1}{n} + 1 \right)} + c_2 \tag{10}$$

where c_2 is the constant of the second integration. The value of c_2 can be determined from the fully developed assumption outlined earlier. In this region the no-slip boundary condition, $u = 0$ is applied at the wall of the channel ($x = h/2$) which leads to:

$$c_2 = -\frac{\left(\frac{h}{2k} \frac{dp}{dx} \right)^{\frac{1}{n}+1}}{\frac{1}{k} \frac{dp}{dx} \left(\frac{1}{n} + 1 \right)} \tag{11}$$

Upon substituting c_2 into Eq. (10) and simplifying the equation, the velocity profile across the channel of the flow can be written as:

$$u(y) = \frac{n}{n+1} \left(\frac{1}{k} \frac{dp}{dx} \right)^{\frac{1}{n}} \left(y^{\frac{n+1}{n}} - \left(\frac{h}{2} \right)^{\frac{n+1}{n}} \right) \tag{12}$$

In order to compare the results at different flow conditions, Eq. (12) can be normalized using the maximum velocity at the centerline of channel to give:

$$\frac{u(y)}{u_{(0,max)}} = 1 - \left(\frac{2y}{h} \right)^{\frac{n+1}{n}} \tag{13}$$

Based on this equation, the normalized velocity of a power law fluid is only a function of the rheological property of the fluid, cross-stream position and channel geometry. The velocity of a Newtonian fluid where $n = 1$ can also be calculated from this equation which simplifies to a parabolic relationship or the common Poiseuille profile [18, 22].

The normalized velocity profiles given in Eq. (13) are plotted for a Newtonian and different non-Newtonian flows as shown in Fig. 2. For a Newtonian fluid ($n = 1$),

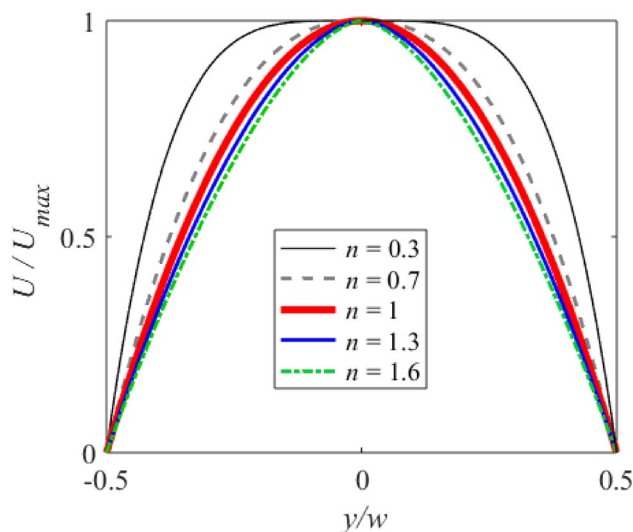


Fig. 2 A comparison of the generated velocity profiles of Newtonian and non-Newtonian flows with different flow indices from the developed mathematical model

the velocity profile shows the expected parabolic/Poiseuille profile [22]. For shear thinning fluids ($n < 1$), the velocity profile approaches a top-hat shape and this shape intensifies as the power law index of the flow decreases. For the case of a shear thickening fluid ($n > 1$), the velocity profile has a sharp-pointed feature at the centerline of the channel. This phenomenon intensifies as the power law index of the fluid increases. The deviations of velocity profile of non-Newtonian fluids from the parabolic shape are due to the variation of the viscosity of the non-Newtonian fluids in the different shear rate regions of the flow. The velocity profiles, in general, become closer to parabolic as the power law index approaches Newtonian behavior ($n = 1$). The result of this analysis highlights that the rheological properties of a fluid can be determined from a well resolved velocity distribution measurement under laminar conditions in a flow channel.

3 Experimental setup

3.1 Sample preparation and rheological measurement of non-Newtonian fluid

To study the effect of fluid rheology on the velocity profile, distilled water and polyacrylamide/water solutions were used as the Newtonian and shear thinning, non-Newtonian fluid, respectively. Polyacrylamide solution was chosen for its transparency as it is required for the velocity measurement using PIV [43]. A shear-thinning fluid was chosen as a representative of non-Newtonian fluid since shear thickening fluids are typically not optically transparent and such fluids commonly resist the movement of particles within. Different concentrations of this solution were also used to determine the effect of variation of the shear-thinning behavior on the velocity profiles. Polyacrylamide solutions were prepared from a commercially available high molecular weight anionic polyacrylamide powder (Magnafloc 5250, BASF SE) with particle size of 1 μm and bulk density of 0.7 g/cm^3 . Anionic polyacrylamide solution was chosen over a cationic one due to its longer stability. Cationic solutions are only stable for a short time (~ 10 min) while anionic solutions are stable for several days [43].

A standard procedure [15] was followed to mix and prepare the solutions. Polyacrylamide powder was gradually added to water while it was mixed at the same time using a magnetic stirrer. In order to have a reliable measurement and avoid the presence of bubbles during flow experiments, prepared samples were degassed using a vacuum pump. The repeatability of the preparation procedure of the solutions was confirmed by measuring the rheology

of different samples of the same concentration [15]. The storage time of polyacrylamide solution were also studied. The prepared solution was kept at room temperature for 30 days during which the rheological properties were measured each day. The mean measured viscosity at different shear rates is shown Fig. 3 and the variations of viscosity over the 30 days are shown as error bars. Based on the results of these measurements, the maximum variation from the mean value was 2.8%. It shows that there was not a significant change in the viscosity of the sample with respect to time, which confirmed that the rheology of polyacrylamide solution was stable for 30 days [15].

The rheological parameters of the solutions shown in Fig. 3 were directly measured using a standard double gap cylinder rheometer (RheolabQC, Anton Paar) with a measuring system (DG42, Anton Paar) having a measuring gap of 0.5 mm. A water bath was connected to the rheometer to maintain constant temperature of the rheological measurements. These measurements were undertaken within the shear rate ($\dot{\gamma}$) range of 10 to 1000 s^{-1} and 360 measurements were recorded for every sample at a rate of 0.1 Hz. The variation of shear rate and shear stress obtained from this measurement were used to determine the rheological properties of the different fluid samples.

Studies on the rheological characteristics of polymer solutions indicated that the viscosity has three different regions of low shear rate plateau, a shear thinning region, and a high shear rate plateau [24]. The measurement of viscosity in the low shear rate plateau region provides the characteristics of the fluid in near-equilibrium conditions. In this region, the calculated viscosity of the fluid is called the zero shear rate viscosity which represents the highest viscosity of the fluid. As the applied shear rate increases, the fluid enters the shear thinning region and the flow shows a power law decrease in the viscosity. The shear thinning region can be described using different models [24]. In engineering applications due to its simplicity, a

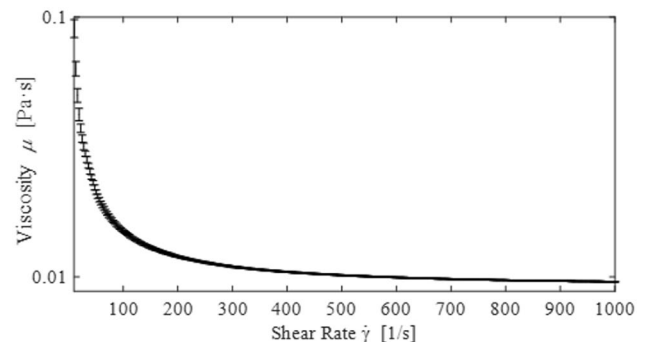


Fig. 3 Rheological measurement of 0.2 wt% polyacrylamide solution using rheometer for 30 measurements collected over the 30 days at 25 °C

power law model is usually used where the viscosity is a function of shear rate and constant values of flow index and consistency. In the high shear rate plateau region, the lowest viscosity can be observed as the polymer chains become disentangled. The viscosity in the high shear rate region is called infinite shear rate viscosity, which is a value close to the solvent viscosity. These three regions can be determined using rheological measurements over a high range of shear rates [24].

Figure 4 shows a sample set of rheological measurement of 0.1 wt% polyacrylamide solution. A linear relationship between the logarithmic scale of viscosity, $\log(\mu)$ and shear rate, $\log(\dot{\gamma})$ was observed as expected for a power law fluid in the shear thinning region. The rheological

parameters of the fluid in the logarithmic scale can be calculated using:

$$\log(\mu) = (n - 1)\log(\dot{\gamma}) + \log(k) \tag{14}$$

$$\log(\tau) = n\log(\dot{\gamma}) + \log(k) \tag{15}$$

The power law index (n) and flow consistency (k) can be determined by curve fitting the rheometer measurements with Eqs. (14) and (15). It can be seen in Fig. 4 there is a variation in slope of the graph with respect to shear rate which represents the deviation of power law index of the fluid in different regions of the measurement. The power law index can be used to classify and divide the rheological measurements into three regions ranges of low shear rate ($1-80 \text{ s}^{-1}$), mid shear rate ($80-160 \text{ s}^{-1}$), and high shear rate ($160-1000 \text{ s}^{-1}$), where each range has different flow indices. The slope of the entire region of the shear rate was chosen as a representative of the power law index of the fluid. The same approach was used to calculate the rheological parameters of the different concentrations of polyacrylamide solutions studied.

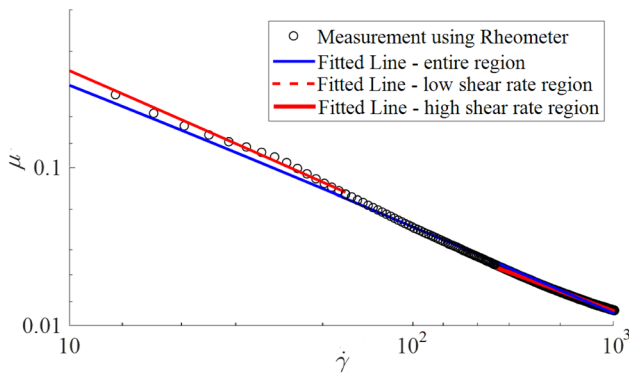


Fig. 4 The variation in viscosity of 0.1 wt% polyacrylamide solution with the change in the shear rate measured using rheometer and fitted curve

3.2 Optical velocity measurement setup

Shadowgraph PIV was used to measure the velocity distributions of the optically transparent fluid as it flowed in a rectangular mini-channel. The setup used for the flow experiments is shown in Fig. 5. The main flow loop included in the setup was made up of a flow chip, a syringe pump and connection tubes. The optical components were a camera, microscopic objective lens, a high current

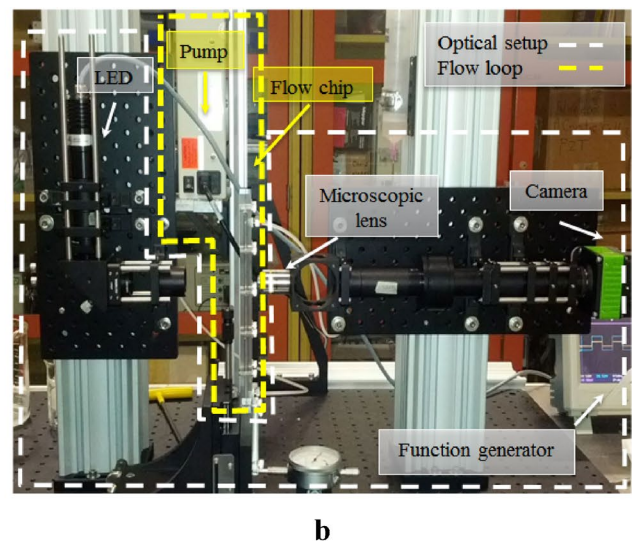
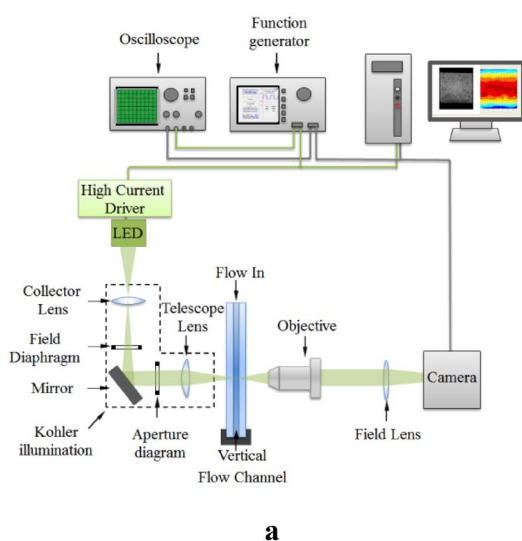


Fig. 5 Experimental setup to study the velocity profile of flow through straight mini-channel: **a** schematic of the setup, and **b** photograph of the setup

LED and a function generator for controlling the timing of events.

In order to study the flow in the desired flow channel, a flow cell was designed as shown in Fig. 6a. This flow cell was made of 3 transparent sheets of PMMA having a thickness of 3.175 mm (Optix; Plaskolit Inc.). Two layers were used as windows for optical measurements while the middle layer was used as the flow channel of a controlled geometry. The rectangular channel was designed to have a 0.69×3.175 mm cross section area and length of 180 mm. To make the required features for all components, a commercial laser cutter (VersaLaser VLS Version 3.50; Universal Laser Systems) was used. The rectangular cross section of the flow channel can be seen in Fig. 6b which shows a closer view of a sectioned assembly.

A syringe pump (PHD 2000; Harvard Apparatus Inc.) was used to inject the fluid to the channel at the required flowrates. The channel was filled from the bottom to prevent the formation of bubbles that would generate extra blockage and interfere with the development of the flow velocity profile. Once a steady flow was attained, measurements were taken from a region in the middle of the channel at a distance beyond the entrance length, which was determined using the Eq. (3). Using the dimensions of the rectangular cross section of the channel, the hydraulic diameter of the channel was 1.14 mm. Since the maximum Reynolds number of this experiment was 10, the longest entrance length needed for the fluid to become fully developed for this channel was 0.62 mm. The region of velocity measurement was selected at 95 mm from the

entrance of the channel to ensure measurement in the fully developed region.

The flow in the channel was determined by tracking the motion of particles seeded into the flow. These seeding particles were made from polystyrene with a mean diameter of $1.0 \mu\text{m}$ (R0100; Thermo Fisher Scientific Company) and were chosen for their uniform size distribution with the bulk density of 1.05 g/cm^3 which matched closely with the densities of water and polyacrylamide solutions. A CMOS camera (SP-5000 M-PMCL-CX; JAI Inc.) with a resolution of 2560×2048 pixels collected images at 90 fps to capture the movement of the seed particles. To have clear images of the particles, a microscopic objective lens with ten times magnification ($\times 10$ MPLN; Olympus Corporation) was used to focus on the width of the mini-channel. The field-of-view of the camera was determined using a target and found to be 1.92×1.55 mm. In this field-of-view, the seeding particles had an average diameter of around 4–5 pixels. This objective lens had a 10.5 mm working distance, depth-of-field of $8.5 \mu\text{m}$ and numerical aperture of 0.25. To insure that the camera was in focus on the mid-plane of the channel, a mechanical dial indicator was used to first determine the extent of the channel and then to control the movement and location of the plane-of-focus.

The particles and flow cell were illuminated using a green high current LED light source (SL112-520 nm; Advanced Illumination Inc.). To correct the uneven distribution of light from the LED, it was coupled with a Köhler illumination [44] configuration shown in Fig. 5a. The camera and LED were operated in a pulse mode in order to freeze the motion of the seeding particles and they were

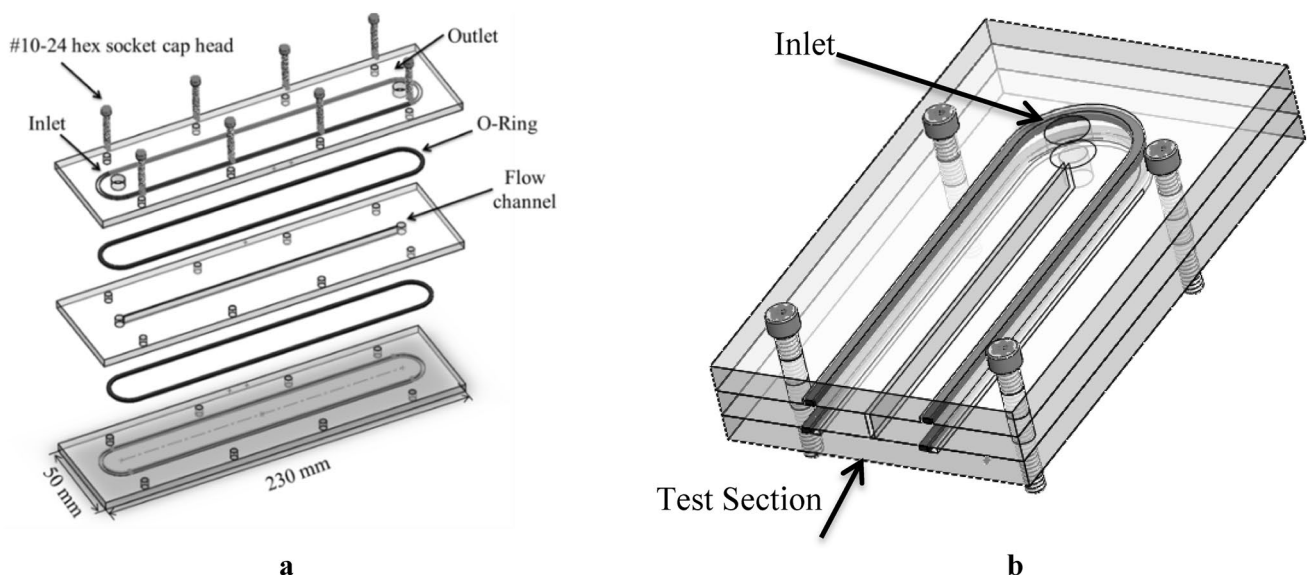


Fig. 6 Flow cell used for analyzing the flow field across the microchannel **a** design of three layers of cell and **b** section view of the channel after assembling

triggered synchronously using continuous square waves from a function generator (AFG3201B; Tektronix Inc.) at a frequency of 90 Hz. At this frequency, the particles in each images moved around 3–4 times of their mean diameter, which confirms that the time interval between images was short enough to freeze the motion of the particles.

3.3 PIV processing of images to velocity fields

Raw images collected via the imaging system were processed using commercial PIV software (DaVis 8.1.4, LaVision GmbH). A preprocessing algorithm was applied to improve image contrast and to normalize the intensity of the raw images. The images were inverted during preprocessing and a non-linear filter and geometric mask were applied to decrease the background noise. After preprocessing, the tracer particles had an average diameter of 2–3 pixels in the images and the displacement between sequential images was between 4 and 5 pixels. A multi-pass sequential cross-correlation algorithm with decreasing window size was then used to determine the velocity vectors from preprocessed images. Square interrogation windows sizes of 64×64 pixels and 32×32 pixels with 87% overlap were used for the first and second passes, respectively. Statistical tools within the software was used for averaging the processed vector fields.

The velocity profiles obtained in this experiment were an average of 200 processed images. In order to plot and compare the results of different conditions, further post processing was applied to the vector field using in-house code (MATLAB, Mathworks Inc.). At this stage the velocity of the fluid and the position along the channel were normalized using the maximum velocity and the entrance width of the channel respectively. Using this data, the velocity profiles and the average velocity vector maps of the fluid at different conditions were plotted in non-dimensional scale. The average velocity vector fields for different solutions at Reynolds number of 1 are shown in Fig. 7. The velocity profiles of

Newtonian fluid as shown in Fig. 7a had a distinct parabolic shape while a top-hat flow profile was found for the shear-thinning fluids as shown in Fig. 7b. When the fluid was shear-thinning the shape of the flow profile showed an increased region of maximum velocity along the width of the channel, approaching a top-hat profile.

3.4 Uncertainty in velocity measurement

Sources of error in PIV experiments have been identified and reported by different studies [44]. Among the sources, distribution of illumination, settling velocity and concentration of tracer particles in the carrying fluid, number of images and PIV processing algorithm have the maximum effect on the PIV measured velocity results. These sources of error need to be addressed and considered to have consistent results.

One of the fundamental assumptions of PIV measurement is that tracer particles faithfully follow the flow of the fluid elements [45]. In order to confirm this fact, the Stokes number can be calculated. Stokes number (St) is a characteristic parameter describing the behavior of suspended particles in a fluid flow. It is defined as the ratio of the relaxation time of a particle (τ_s) to a characteristic time of the flow ($\frac{u_o}{l_o}$):

$$St = \frac{\tau_s u_o}{l_o}$$

where u_o is the fluid velocity and l_o is the characteristic length scale and in this case the width of channel. In case of spherical particles in a viscous laminar flow, the relaxation time is:

$$\tau_s = \frac{1}{18} \frac{\rho_p D_p^2}{\mu_p}$$

where ρ_p and D_p are density and diameter of the particle respectively.

Resulting in:

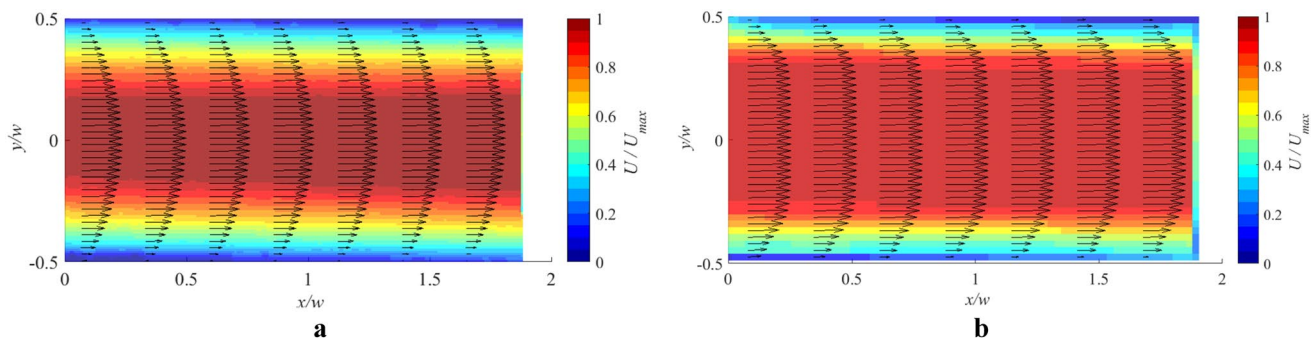


Fig. 7 Average velocity profile vector plot with a background color map of velocity magnitude for **a** water, and **b** 0.4 wt% polyacrylamide, through mini-channel at $Re = 1$

$$St = \frac{1}{18} \frac{\rho_p D_p^2 u_o}{\mu_p l_o}$$

Therefore, the Stokes number in this study of tracer particles ($D_p = 2 \times 10^{-6}$ m, $\rho_p = 1.05 \times 10^6$ kg/m³) suspended in water ($\mu_f = 0.000891$ kg/m s) with the average velocity of the fluid ($u_o \sim 7$ mm/s) was calculated to be 1.83×10^{-3} . As $St \ll 1$, it can be concluded that the motion of the flow can be determined from the movement of the tracer particles [35].

To identify the required number of images to have a consistent result, a convergence plot of the flow of water at the highest Reynolds number ($Re = 10$) was generated. Based on these results, the average velocity becomes a constant value for the average after 100 images. This indicates that the number of images collected was sufficient to describe the velocity of the fluid. It is reported that an estimate for the overall uncertainty of the velocity measurements using PIV is between 0.05 to 0.1 pixels [46, 47]. Converting this variation from pixel space to physical space and using the frame rate of the camera, the maximum variation is 6.75×10^{-3} mm/s. The uncertainty of the velocity is approximately within the range of 0.1% with respect to average velocity of the fluid (~ 7 mm/s) at $Re = 10$.

4 Results and discussion

4.1 Standard measurement of rheological properties

The variation in the viscosity and shear stress with respect to changes in the applied shear rate measured using a

rheometer for different concentrations of polyacrylamide solution are shown in Fig. 8. The results indicated that the viscosity of the polyacrylamide solutions decreased as the shear rate increased which reflected the shear-thinning behavior of the fluid for the range of the shear rate considered. It is also observed that the viscosity of polyacrylamide solutions increased as the concentration of the sample increased. Shear thinning behavior was observed for all concentrations of polyacrylamide solutions. The variation of the viscosity with respect to shear rate became more significant as the concentration of polyacrylamide solution increased. This represents the dominance of the shear thinning behavior of the fluid. Measurements of the viscosity distributions were triplicated in order to check the repeatability of the measurements. Only 1% variation in the viscosity of the fluid was seen in the results of rheological measurements.

Figure 9 shows the variation of the viscosity with respect to shear rate on a log–log scale for the different polyacrylamide solutions. Based on Eq. (13), the power law index of the fluid can be calculated using the slope of this graph. It can also be seen in the figure that there is a variation in the slope of the graph with respect to shear rate for some solutions. The slope of the graph is smaller at low shear rates and it increases at high shear rates, which indicates the variation of the power law index of the fluid as the shear rate changes. In order to generally compare the results, the slope of the rheological measurement curves in Fig. 9 within the shear rate ($\dot{\gamma}$) range of 10–1000 s⁻¹ were used to determine the power law index, n , of the fluid. The flow indices of the polyacrylamide solutions of different concentrations were calculated using a power law model of Eq. (1) and the results are summarized in Table 1. The plots corresponding to

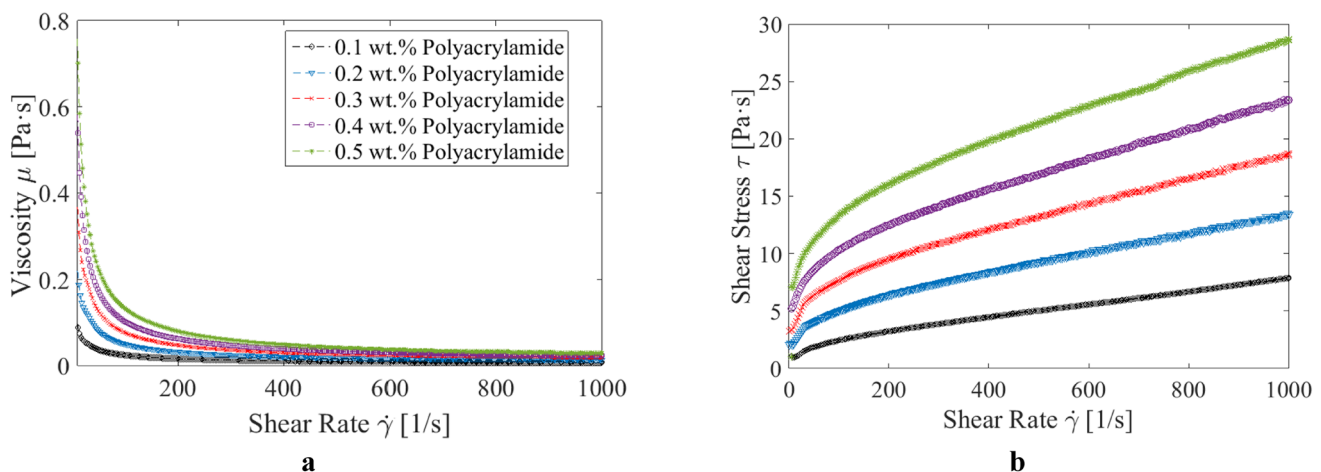


Fig. 8 Rheological measurements of polyacrylamide solution using a rheometer at 25 °C **a** variations in the viscosity, and **b** shear stress with respect to change in the shear rate for different concentration of solution

Fig. 9 Viscosity measurements of polyacrylamide solution using a rheometer at 25 °C at different shear rates

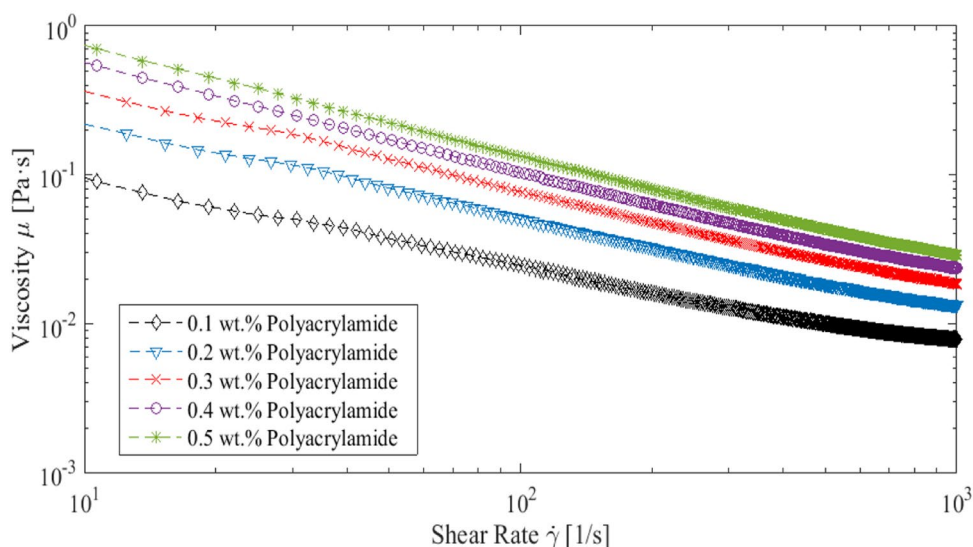


Table 1 Rheological parameters for different concentrations of polyacrylamide solution using Ostwald de Waele power law model

Solution concentration	Power law index (<i>n</i>)	Flow consistency (<i>k</i>)
0.1 wt% polyacrylamide	0.47	0.054
0.2 wt% polyacrylamide	0.38	0.813
0.3 wt% polyacrylamide	0.33	3.115
0.4 wt% polyacrylamide	0.32	7.112
0.5 wt% polyacrylamide	0.26	11.61

these results are shown in Fig. 10 to give better clarity for comparison along with minimum and maximum shear rates using the approach shown in Fig. 4 to give a range of expected values. The power law index, *n*, decreased as the concentration of the polyacrylamide solution increased. The decrement of the power law index of the fluid indicated that the shear thinning behavior of the

fluid intensified as the concentration of polyacrylamide in the fluid increased.

The relation between the power law index, *n*, and flow consistency, *k*, with respect to the concentration of polyacrylamide solution in the range of measurement were determined using the rheological measurements represented in Fig. 10. These are listed in Table 2 where *C* is the concentration of the polyacrylamide solution in wt% of the water solution.

4.2 Velocity profile of Newtonian and non-Newtonian fluid through narrow straight channel

The effect of the shear-thinning behavior of the polyacrylamide solution as compared to the Newtonian behavior of water on the shape of velocity profile was identified by plotting the velocity profiles of all solutions at the same *Re* and location along the channel as shown

Fig. 10 Variation in power law index (*n*) and flow consistency (*k*) determined using the rheometer with the change in concentration of polyacrylamide solution

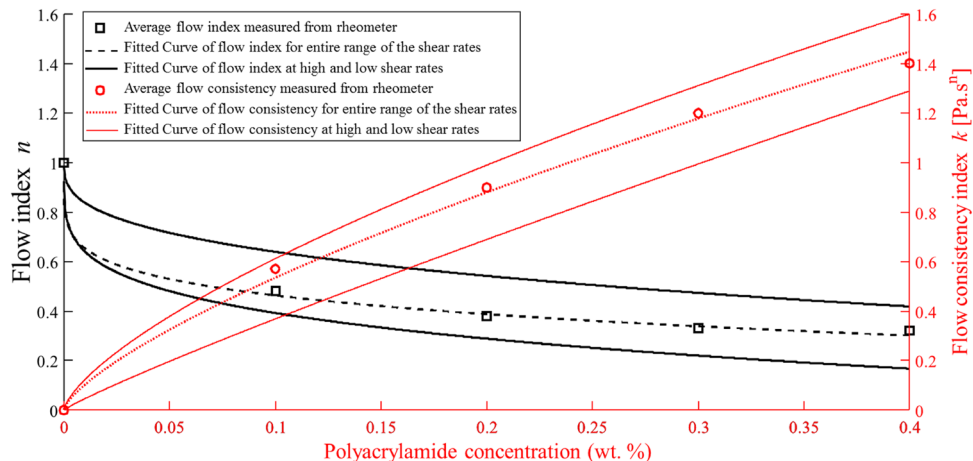


Table 2 Curve fitted equation of the power law index and flow consistency with respect to concentration of polyacrylamide solution at different ranges of shear rate

Low shear rate	Entire range of shear rate	High shear rate
$n = 1 - 0.933(C)^{0.227}$	$n = 1 - 0.831(C)^{0.195}$	$n = 1 - 0.7964(C)^{0.344}$
$k = 2.282(C)^{0.904}$	$k = 2.955(C)^{0.7102}$	$k = 3.021(C)^{0.696}$

in Fig. 11. The velocity is normalized by the maximum velocity through the channel and the position is normalized by the width of the channel to compare results from different flow conditions. The graphs indicated that water has a parabolic velocity profile and the velocity profile approaches a top-hat shape as the concentration of the polyacrylamide solution increases. This result shows that the shear thinning behavior of the fluid intensifies as the concentration of the polyacrylamide increases. Increase in the concentration of polyacrylamide powder in a solution will result in the increase of the dominance of the intermolecular forces that bring about the non-Newtonian properties. This phenomenon was observed at all *Re* values considered in this study.

To find the power law index of the fluid, the average of normalized velocity profiles were fitted to the power law model:

$$\frac{u}{u_{max}} = a\left(\frac{y}{w}\right)^b + c \tag{16}$$

This equation can represent the variables in Eq. (13) only if $c = 1$ and a and b are defined as:

$$\frac{a}{c} = (-2)^{\frac{n+1}{n}} \tag{17}$$

$$b = \frac{n + 1}{n} \tag{18}$$

The power law index could thus be found by comparing the non-linear fitted data using commercial software (MATLAB, Mathworks Inc.) with corresponding theory.

The validity of the above model can be seen in the example result in Fig. 12 which shows a case where the velocity profile of 0.2 wt% polyacrylamide solution at *Re* = 1 is fitted to the power law model given by Eq. (17). The calculated power law index for this solution confirms the non-Newtonian behavior of the flow ($n = 0.36$) which has a good agreement with the rheometer measurements ($n = 0.38$). The same approach was used to calculate the flow indices for different concentrations of polyacrylamide solution at different Reynolds numbers. Three sets of data were considered for each condition and an average of all flow indices was determined with a standard deviation of 0.015 is presented in Table 3. The power law index decreased as the concentration of polyacrylamide solution increased which shows the increase in non-Newtonian behavior of the fluid. The power law index also increased as *Re* increased.

In order to validate the results of the PIV measurements, the flow indices from velocity profile measurement results were compared with rheological properties of the fluid determined from the rheometer. Due to the strong effect of temperature on the rheological properties of the fluid, the rheological measurements were taken at the same temperature of the flow study ($T = 20^\circ\text{C}$). The flow indices of the fluid given by the fitted functions of the rheometer measurements in Table 2 and experimentally determined values using shadow PIV in Table 3 are plotted in Fig. 13 for comparison. The solid lines represent the range of the flow indices measured from the rheometer. The average of the entire range of measurements using the rheometer is also

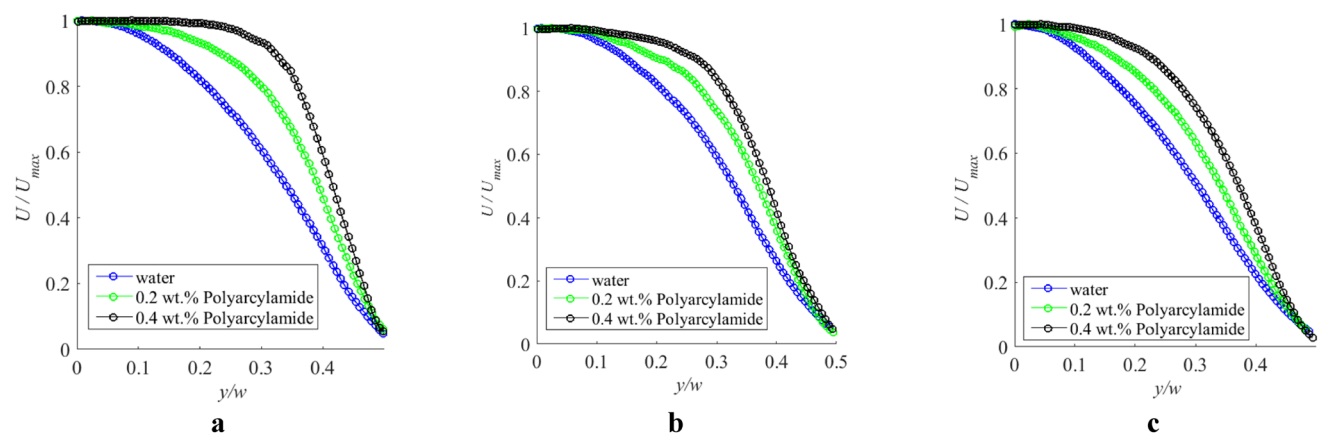


Fig. 11 Measured velocity profiles showing the effect of Newtonian and non-Newtonian behavior of a fluid on the shape of velocity profile at **a** *Re* = 0.1, **b** *Re* = 1 and **c** *Re* = 10

Fig. 12 A plot of curve-fitted data showing the validity of the model developed in the present study **a** water and **b** 0.2 wt% Polyacrylamide at $Re = 1$

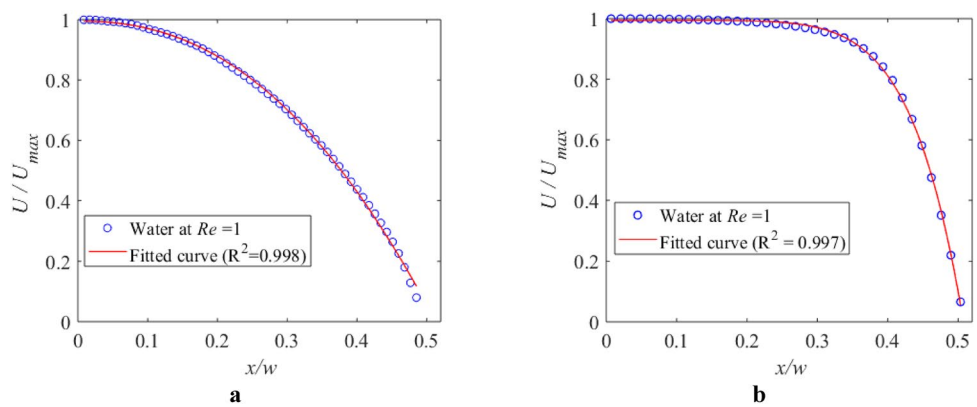
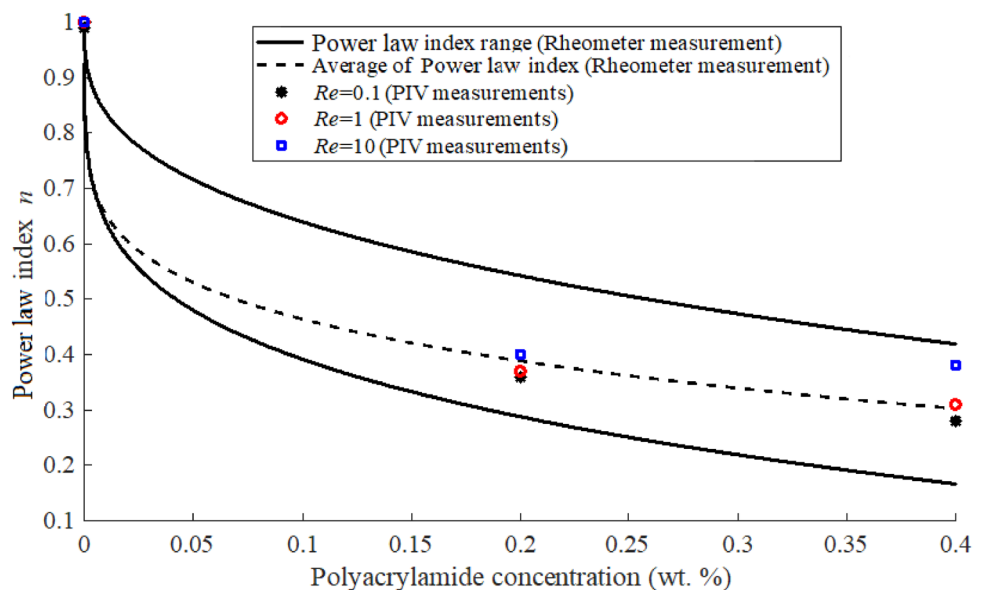


Table 3 The average of power law index for different concentrations of Newtonian and shear-thinning solution determined from three measured velocity profiles for each case

Fluid	Re	Power law index (n) PIV measurement	Power law index (n) Rheometer
Water	0.1	0.99	1
	1	1	
	10	1	
0.2 wt% polyacrylamide	0.1	0.36	0.38
	1	0.37	
	10	0.40	
0.4 wt% polyacrylamide	0.1	0.30	0.32
	1	0.34	
	10	0.39	

shown for comparison. Results indicate that, at all Reynolds numbers, flow indices for polyacrylamide solutions from PIV measurements and from rheometer measurements lie in the same range. The power law index at $Re = 1$ and the average power law index calculated using the rheometer are in good agreement. It should be noted that the average of the power law index of the fluid reported from rheometer measurements was found based on the slope of the entire range of the shear rate measurements. The power law index calculated from velocity profiles of the polyacrylamide solution is higher at higher Re numbers and the same trend was observed from measurements from the rheometer. This plot indicates that the highest variation exists for higher Re numbers and concentrations of polyacrylamide were the shear thinning behavior of the fluid increases. Based on these measurements, it can be concluded that the shear thinning behavior of the fluid is more dominant at lower Re numbers.

Fig. 13 Comparison of power law index of polyacrylamide solution determined from PIV and rheometer measurement



The velocity profiles at different Re were compared with Newtonian and non-Newtonian theories to study the effect of rheology on the shape of the resultant velocity profiles. The plots of the velocity profiles at different flow rates and respective theories using the measured flow indices are shown in Fig. 14. As it is shown in Fig. 14a, Re had no effect on the shape of the Newtonian velocity profile due to the constant power law index of the Newtonian fluid as shown in Table 1. For shear-thinning fluids, however, the top-hat shape in the velocity profile became less visible as Re increased and this condition was confirmed by the increment of power law index seen in Table 1. These results implied that at low Re , where the shear rate is lower, the non-Newtonian behavior intensifies while at higher shear rate the Newtonian behavior of the fluid is more dominant.

5 Conclusion

The velocity profiles of Newtonian and shear-thinning fluids were obtained using shadowgraph PIV. For the case of Newtonian fluid, a parabolic profile was observed as expected following the theory of Poiseuille flows. The velocity profile of shear-thinning fluids had a top-hat shape and as the non-Newtonian behavior of the fluid became dominant with increasing shear, the top-hat profile became more visible. By curve fitting the velocity profile obtained from experiments to the corresponding theory, the power law index of the fluid could be determined for different concentrations of polyacrylamide solution and different Reynolds numbers.

The comparison of the results of Newtonian and non-Newtonian fluids reflected that the shear thinning behavior of the fluid leads to a top-hat velocity profile.

Increase in Reynolds number resulted in the change in the rheological behavior of the fluid. The shear thinning behavior of the fluid intensified at lower Reynolds numbers where lower shear rates prevailed at the walls. Increasing the Reynolds number also increased the power law index of the fluid resulting in a weaker non-Newtonian behavior of the fluid. The result of the increment of the power law index showed the same trend that was expected from rheological measurements.

The study presented in this paper showed that the flow index of a Newtonian and shear-thinning fluid can be identified using experimentally obtained velocity profile data. The key to the approach introduced here was fitting experimental data to the developed model for Newtonian and non-Newtonian flows through mini-channels to determine the power law index. Utilizing a PIV flow measurement technique ensured non-intrusive and in-situ measurement of a fluid's rheology. This method will enable the fluid's viscosity variation as per change in shear rate can be done for any flowrate within the creeping and laminar flow regions.

Although the current study is based on the flow index of Newtonian and shear thinning fluids, the findings suggest that the application can be used in any range of temperature and pressure that are specific to the flow scenarios found in the application. This capability ensures that the flow properties are more representative of the real application. Whereas in the case of using a conventional rheometer, it can be unclear whether the applied shear rate during the rheometer measurement actually corresponds to the conditions that the fluid maybe experiencing in the actual flow situation. The non-intrusive nature of the measurement also enables the measurement the flow behavior index of any fluid despite their chemistry and physical properties. Taken together, this method can

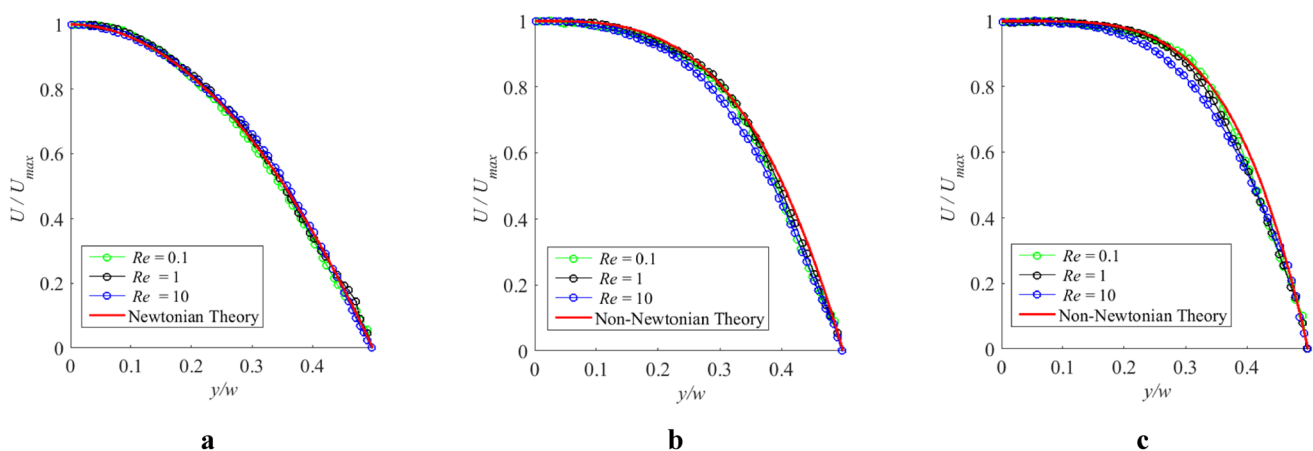


Fig. 14 Velocity profiles of **a** water, **b** 0.2 wt% polyacrylamide and **c** 0.4 wt% polyacrylamide at different Re numbers with their corresponding theory

be used as an in-situ rheological measurement where the rheological behavior of the fluid can be determined without any previous knowledge of the fluid and its behavior in real case scenario.

The findings in this paper have focused on the specific conditions of a transparent Newtonian and non-Newtonian passing through a mini-channel. The application of the method can be extended to future applications. First, the PIV approach used in this study requires a transparent fluid which is not exist in all applications. The introduced methodology can be used to study an opaque fluid by utilizing methods such as X-ray PIV. Future studies on the current topic are therefore recommended. Secondly, the flow index of the fluid was determined in mini-channels. The application of this study can be also extended to micro and macro scale applications. Thirdly, the study did not evaluate the rheology of shear thickening fluids. Further research should be done to investigate the validity of the application for these fluids.

Author contributions Optional: please review the submission guidelines from the journal whether statements are mandatory.

Funding Natural Sciences and Engineering Research Council (NSERC) of Canada, the Alberta Ingenuity Fund, the Canadian Foundation for Innovation (CFI) and RGL Reservoir Management Inc..

Availability of data and materials Data transparency.

Code availability Not applicable.

Compliance with ethical standards

Conflicts of interest The authors declare that they have is no conflict of interest.

References

1. Khodaparast S, Borhani N, Thome JR (2014) Sudden expansions in circular microchannels: flow dynamics and pressure drop. *Microfluid Nanofluid* 17(3):561–572. <https://doi.org/10.1007/s10404-013-1321-7>
2. Nakano M (2000) Places of emulsions in drug delivery. *Adv Drug Deliv Rev* 45(1):1–4
3. Akoglu, E. (2007). Measurement instrumentation sensors Handbook, vol 104. CRC Press LLC. <https://doi.org/10.1073/pnas.0703993104>
4. Kandlikar SG (2006) Single-phase liquid flow in minichannels and microchannels. In: Heat transfer and fluid flow in minichannels and microchannels, pp 87–133
5. Li D, Xuan X (2018) Fluid rheological effects on particle migration in a straight rectangular microchannel. *Microfluid Nanofluid*. <https://doi.org/10.1007/s10404-018-2070-4>
6. Ansari S, Yusuf Y, Kinsale L, Sabbagh R, Nobes DS (2018) Visualization of fines migration in the flow entering apertures through the near-wellbore porous media. *SPE*, SPE-193358
7. Mezger TG (2011) The rheology handbook, 3rd edn. Vincentz Network, Hannover
8. Macosko CW (1994) Rheology principles, measurements and applications. VCH Publishers, New York
9. Hou YY, Kassim HO (2005) Instrument techniques for rheometry. *Rev Sci Instr* 10(1063/1):2085048
10. Yang S, Ji B, Ündar A, Zahn JD (2006) Microfluidic devices for continuous blood plasma separation and analysis during pediatric cardiopulmonary bypass procedures. *ASAIO J* 52(6):698–704. <https://doi.org/10.1097/01.mat.0000249015.76446.40>
11. Ansari S, Sabbagh R, Yusuf Y, Nobes DS (2019) The role of emulsions in oil-production process : a review. *SPE Journal*, (March), 1–21. Retrieved from <https://doi.org/10.2118/199347-PA>
12. Beebe DJ, Mensing GA, Walker GM (2002) Physics and applications of microfluidics in biology. *Annu Rev Biomed Eng* 4(1):261–286. <https://doi.org/10.1146/annurev.bioeng.4.112601.125916>
13. Han Y, Liu Y, Li M, Huang J (2012) A review of development of micro-channel heat exchanger applied in air-conditioning system. *Energy Procedia* 14:148–153. <https://doi.org/10.1016/j.egypro.2011.12.910>
14. Terzopoulos D (1984) Advances in computational vision and medical image processing, vol 13. Springer, Berlin
15. Ansari, S. (2016). Newtonian and non-Newtonian flows through mini-channels and micro-scale orifices for SAGD applications. MSc thesis, University of Alberta.
16. Cross MM (1965) Rheology of non-Newtonian fluids: A new flow equation for pseudoplastic systems. *J Colloid Sci* 20(5):417–437. [https://doi.org/10.1016/0095-8522\(65\)90022-X](https://doi.org/10.1016/0095-8522(65)90022-X)
17. Irgens F (2013) Rheology and non-Newtonian fluids. Springer, Springer. <https://doi.org/10.1007/978-3-319-01053-3>
18. Westerhof N, Stergiopoulos N, Noble MIM (2010) Law of Poiseuille. In: Snapshots of hemodynamics. Springer, Berlin. <https://doi.org/10.1007/978-1-4419-6363-5>
19. Fu T, Carrier O, Funfschilling D, Ma Y, Li HZ (2016) Newtonian and Non-Newtonian flows in microchannels: inline rheological characterization. *Chem Eng Technol* 39(5):987–992. <https://doi.org/10.1002/ceat.201500620>
20. Chhabra RP (2010) Non-Newtonian fluids: an introduction. *Rheol Complex Fluids*. https://doi.org/10.1007/978-1-4419-6494-6_1
21. Bingham EC (1922) Fluidity and plasticity:engineering, 5th edn. McGraw Hill Book Company Inc., New York. <https://doi.org/10.1017/CBO9781107415324.004>
22. Kundu PK, Cohen IM (2002) Fluid mechanics, 2nd edn, vol 80. Academic Press, Cambridge. ISBN 978-0-12-381399-2
23. Tropea EC, Yarin AL, Foss JF (2007) Springer handbook of experimental fluid mechanics. <https://doi.org/10.1007/978-3-540-30299-5>
24. Vazquez M, Schmalzing D, Matsudaira P, Ehrlich D, Mckinley G (2001) Shear-induced degradation of linear polyacrylamide solutions during pre-electrophoretic loading. *Anal Chem* 73(13):3035–3044
25. Mason TG, Weitz DA (1995) Optical measurements of frequency-dependent linear viscoelastic moduli of complex fluids. *Phys Rev Lett* 74:1250–1253
26. Nordstrom KN, Verneuil E, Arratia PE, Basu A, Zhang Z, Yodh AG, Gollub JP, Durian DJ (2010) Microfluidic rheology of soft colloids above and below jamming. *Phys Rev Lett* 105:1–4. <https://doi.org/10.1103/PhysRevLett.105.175701>
27. Completo C, Geraldes V, Semiao V (2010) Micro-PIV characterization of laminar developed flows of Newtonian and non-Newtonian fluids in a slit channel. *Proc Intl Conf Exp Fluid Mech* 19(1):87–97
28. Brandestini M (1976) A digital 128-channel transcutaneous blood flow meter. *Biomed Tech* 21(s1):291–293

29. Wiklund J, Shahram I, Stading M (2007) Methodology for in-line rheology by ultrasound Doppler velocity profiling and pressure difference techniques. *Chem Eng Sci* 62:4277–4293. <https://doi.org/10.1016/j.ces.2007.05.007>
30. Kotzé R, Haldenwang R, Fester V, Rössle W (2014) A feasibility study of in-line rheological characterisation of a wastewater sludge using ultrasound technology. *Water SA* 40(4):579–586
31. Wiklund J, Stading M, Trägårdh C (2007) Ultrasound Doppler based In-line rheometry for processing applications. *Ann Trans Nordic Rheol Soc* 15:1–2
32. Bruun HH (1995) Hot-wire anemometry: principles and signal analysis. *Meas Sci Technol* 7(10):532. <https://doi.org/10.1088/0957-0233/7/10/024>
33. Jensen KD (2004) Flow measurements techniques. *J Braz Soc Mech Sci Eng* 26(4):400–419. <https://doi.org/10.1590/S1678-58782004000400006>
34. Klopfenstein R Jr (1998) Air velocity and flow measurement using a Pitot tube. *ISA Trans* 37(4):257–263. [https://doi.org/10.1016/S0019-0578\(98\)00036-6](https://doi.org/10.1016/S0019-0578(98)00036-6)
35. Raffel M, Willert CE, Kompenhans J (2007) 211 Fluid mechanical properties. In: *Particle image velocimetry: a practical guide*, 2nd edn. Springer, Berlin, vol 49, pp 15–16
36. Fouras A, Kitchen MJ, Dubsy S, Lewis RA, Hooper SB, Hourigan K (2009) The past, present, and future of x-ray technology for in vivo imaging of function and form. *J Appl Phys* 10(1063/1):3115643
37. Heindel TJ (2011) A review of X-ray flow visualization with applications to multiphase flows. *J Fluids Eng* 133(7):074001. <https://doi.org/10.1115/1.4004367>
38. Heindel TJ, Gray JN, Jensen TC (2008) An X-ray system for visualizing fluid flows. *Flow Meas Instrum* 19(2):67–78. <https://doi.org/10.1016/j.flowmeasinst.2007.09.003>
39. Im K-S, Fezzaa K, Wang YJ, Liu X, Wang J, Lai M-C (2007) Particle tracking velocimetry using fast x-ray phase-contrast imaging. *Appl Phys Lett* 90(9):091919. <https://doi.org/10.1063/1.2711372>
40. Lee SJ, Kim GB (2003) X-ray particle image velocimetry for measuring quantitative flow information inside opaque objects. *J Appl Phys* 94(5):3620–3623. <https://doi.org/10.1063/1.1599981>
41. Yim D, Kim GB, Kim D, Lee H, Lee SJ (2007) Medical X-ray PIV technique for visualizing quantitative velocity field distributions of blood flows. *IFMBE Proc* 14/2(14):742–745
42. Kozicki W, Chou CH, Tiu C (1966) Non-Newtonian flow in ducts of arbitrary cross-sectional shape. *Chem Eng Sci* 21(8):665–679. [https://doi.org/10.1016/0009-2509\(66\)80016-7](https://doi.org/10.1016/0009-2509(66)80016-7)
43. Fang L, Brown W, Koňák Č (1990) Dynamic properties of polyacrylamide gels and solutions. *Polymer* 31(10):1960–1967. [https://doi.org/10.1016/0032-3861\(90\)90024-S](https://doi.org/10.1016/0032-3861(90)90024-S)
44. Benner G, Probst W (1994) Köhler illumination in the TEM: fundamentals and advantages. *J Microsc* 174(3):133–142. <https://doi.org/10.1111/j.1365-2818.1994.tb03461.x>
45. Adrian RJ (1991) Particle-imaging techniques for experimental fluid mechanics. *Annu Rev Fluid Mech* 23(1):261–304. <https://doi.org/10.1146/annurev.fl.23.010191.001401>
46. Wieneke B (2015) PIV uncertainty quantification from correlation statistics. *Meas Sci Technol* 26(7):7–10. <https://doi.org/10.1088/0957-0233/26/7/074002>
47. Xue Z, Charonko J, Vlachos P (2013) Signal-to-noise ratio, error and uncertainty of PIV measurement. In: 10th International symposium on particle image velocimetry. Retrieved from https://repository.tudelft.nl/assets/uuid:a6270b28-1132-4186-817e-259eef0e9d87/A093_Xue_Charonko_Vlachos.pdf

Publisher's Note Springer Nature remains neutral with regard to jurisdictional claims in published maps and institutional affiliations.